EUROFUSION WPPFC-PR(16) 14634

Y Marandet et al.

Assessment of the effects of Scrape-off layer fluctuations on first wall sputtering with the TOKAM-2D turbulence code

Preprint of Paper to be submitted for publication in
Plasma Physics and Controlled Fusion

This work has been carried out within the framework of the EUROfusion Consortium and has received funding from the Euratom research and training programme 2014-2018 under grant agreement No 633053. The views and opinions expressed herein do not necessarily reflect those of the European Commission.

Assessment of the effects of Scrape-off layer fluctuations on first wall sputtering with the TOKAM-2D turbulence code

Y. Marandet[a], N. Nace[b], M. Valentinuzzi[b], P. Tamain[b], H. Bufferand[b], G. Ciraolo[b], P. Genesio[a] and N. Mellet[a]

[a] Aix-Marseille Université, CNRS, PIIM, UMR 7345, Marseille, France
[b] CEA, IRFM, F-13108 Saint-Paul-Lez-Durance, France

E-mail: yannick.marandet@univ-amu.fr

November 2015

Abstract. Plasma material interactions on the first wall of future tokamaks such as ITER and DEMO are likely to play an important role, because of turbulent radial transport. The latter results to a large extent from the radial propagation of plasma filaments through a tenuous background. In a such a situation, mean field descriptions (on which transport codes rely) become questionable. First wall sputtering is of particular interest, especially in a full W machine, since it has been shown experimentally that first wall sources control core contamination. In ITER, beryllium sources there will be one of the important actors in determining the fuel retention level through codeposition. In this work, we study the effect of turbulent fluctuations on mean sputtering yields and fluxes, relying on a new version of the TOKAM-2D code which includes ion temperature fluctuations. We show that fluctuations enhance sputtering at near threshold energies, by more than order of magnitude in some cases. This requires higher fluctuation levels than those observed in TOKAM-2D, in particular on ion temperature, which however fit within the range of what has been reported experimentally.

1. Introduction

Burning plasmas require low level of impurities in the core, because of fuel dilution (low Z impurities) and/or radiation losses (high Z impurities, in particular tungsten W) [1]. The fuel retention issue has been the major drive behind the shift from carbon to tungsten in the ITER divertor [2, 3]. This change back to metallic walls, which had been mostly abandoned in the eighties because of unacceptably high plasma contamination, is made possible by low plasma temperatures achieved in divertor configurations (down to less than 1 eV). The sputtered W flux, even by impurities, is expected to essentially vanish in the inter-ELMs (Edge Localized Modes) phase. Recent works suggest that because of plasma conditions during ELMs (high density $\sim 10^{21}\mathrm{m}^{-3}$ and high temperatures $T_e \sim 100$ eV), prompt redeposition could reduce sputtered fluxes by a factor of

the order of 10^4 [4, 5]. As a result, divertor W sources might turn out not to be a real issue in ITER or in DEMO. One of the first drive to build divertor configurations was to localize plasma wall interactions far from the confined plasma, in order to limit impurity contamination. In that respect, divertors are a mixed success because of upstream impurity ions transport in the SOL (Scrape-off Layer), essentially by thermal forces, but also because interactions with the first wall are not fully avoided [6]. In this work we focus on the latter, which are related to the nature of turbulent radial transport in the SOL, exhibiting ballistic-like propagation of filaments [1]. This leads to long e-folding lengths far from the separatrix, hence to significant interactions with the wall. In ITER, first wall erosion determines the plasma content in Beryllium, hence the level of co-deposition. In a full-W DEMO, first wall erosion could be a major determinant of the overall W concentration in the discharge. In fact, experiments in AUG strongly suggest that first wall sources provide the dominant contribution to plasma contamination (i.e. to the W concentration in the core) [7]. While SOL impurity screening clearly plays a role in this, Soledge2D-EIRENE [8] mean field modeling also points towards the role of prompt-redeposition, which is mostly immaterial for the first wall (because of plasma conditions there) [9]. Fluctuations could be an additional important player here because physical sputtering occurs above an energy threshold, so that fluctuations should lead to non-zero sputtering even in conditions for which the mean impact energy is below the threshold. Here, we focus on the role of plasma fluctuations on the mean (that is, time averaged) sputtered fluxes. These are the relevant quantities for mean field models, that is transport codes (such as SOLPS4.x [10], SOLPS5.x [11], EDGE2D-EIRENE [12, 13], UEDGE [14], SONIC [15] and more recently SolEdge2D-EIRENE), but also for spectroscopic measurements of erosion via the S/XB technique (see e.g. [16] for a recent exemple), where turbulent fluctuations are generally not resolved in time. The limitations of mean field models when dealing with non linear functions of the plasma parameters have been highlighted by several authors in the past [17, 18, 19, 20]. The basics of sputtering yield calculations is summarized in Sec. 2, where we introduce in particular the velocity distribution in the parallel direction (that is, along the magnetic field). A new version of the TOKAM-2D turbulence code, including an equation for ion temperature, is presented in Sec. 3, together with a characterization of the fluctuations obtained. Finally, the effects of these fluctuations on sputtering are discussed in Sec. 4, by comparing mean sputtered fluxes to sputtered fluxes calculated with the mean fields. Conclusion and perspectives are outlined in Sec. 6.

2. Sputtered fluxes

In this section, we discuss the basics for the calculation of sputtered fluxes. Physical sputtering can be characterized by a yield $Y_{\mathcal{P}\to\mathcal{T}}$, where $\mathcal{P}$ stands for Projectile and $\mathcal{T}$ for Target, such that

$$\Gamma_{\mathcal{T}} = Y_{\mathcal{P}\to\mathcal{T}}\Gamma_{\mathcal{P}}, \tag{1}$$

	$E_b(eV)$	γ	$E_{th}(eV)$	$E_{TF}(eV)$	Q
Be	3.38	6.0×10^{-1}	13.09	282	0.11
W	8.68	4.3×10^{-2}	209.37	9925	0.07

Table 1. parameters in Bohdansky's formula for sputtering yields, for D on Be and on W

with $\Gamma_{\mathcal{P}}$ the incident projectile flux and $\Gamma_{\mathcal{T}}$ the sputtered flux. For a given combination of projectile and targets, the yield depends on the incident energy E of the projectiles as well as on their incidence angles α_I with respect to the surface normal, namely $Y_{\mathcal{P}\to\mathcal{T}} = Y_{\mathcal{P}\to\mathcal{T}}(E, \alpha_I)$. We expect that turbulent fluctuations will affect more strongly the incident energy than the incidence angle, so that in the following we shall assume that α_I is fixed (actually, we consider that $\alpha_I = 0°$, normal incidence). The behavior of the sputtering yield with energy is well described by the modified Bohdansky formula [21],

$$Y_{\mathcal{P}\to\mathcal{T}}(E, \alpha_I = 0) = Q S_n \left(\frac{E}{E_{TF}}\right)\left(1 - \left(\frac{E_{th}}{E}\right)^{2/3}\right)\left(1 - \left(\frac{E_{th}}{E}\right)\right)^2, \quad (2)$$

where Q is the yield factor, S_n the nuclear stopping cross section, given by

$$S_n(x) = \frac{3.441\sqrt{x}\ln(x + 2.718)}{1 + 6.355\sqrt{x} + x(6.882\sqrt{x} - 1.708)}, \quad (3)$$

with $x = E/E_{TF}$. The Thomas-Fermi energy E_{TF} depends on the combination of target/projectiles, and the threshold energy E_{th} can be written as $E_{th} = E_B/(\gamma(1-\gamma))$, where E_B is the surface binding energy and γ the maximum energy fraction transferred during a collision, $\gamma = 4M_{\mathcal{T}}M_{\mathcal{P}}/(M_{\mathcal{T}} + M_{\mathcal{P}})^2$. Table 2 shows the parameters pertaining to Deuterium impinging on beryllium (Be) and tungsten (W). The yields calculated with these parameters are plotted on Fig. 2 a) as a function of energy. The steep variation of the yield in the threshold region suggests that energy fluctuations could have a strong impact on the mean (time averaged) yields. This statement is made more quantitative on Fig. 2 b), which shows the relative fluctuation amplification factor defined as

$$F = \frac{dY/Y}{dE/E} = \frac{d\ln Y}{d\ln E}. \quad (4)$$

It should be highlighted that F is the highest for energies at which the sputtering yield is the lowest. Note also that time scales associated to physical sputtering are very fast ($\sim 10^{-12}$ s) compared to those characterizing turbulence ($\sim 10^{-6}$ s), so that the model presented in this section is still valid at turbulent scales.

Next, we specify how the impact energy E relates to plasma conditions. In the following, we consider that the plasma is made of one species of fuel atoms (e.g. deuterium), and possibly contains impurities at trace level, with charge Z. The simplest

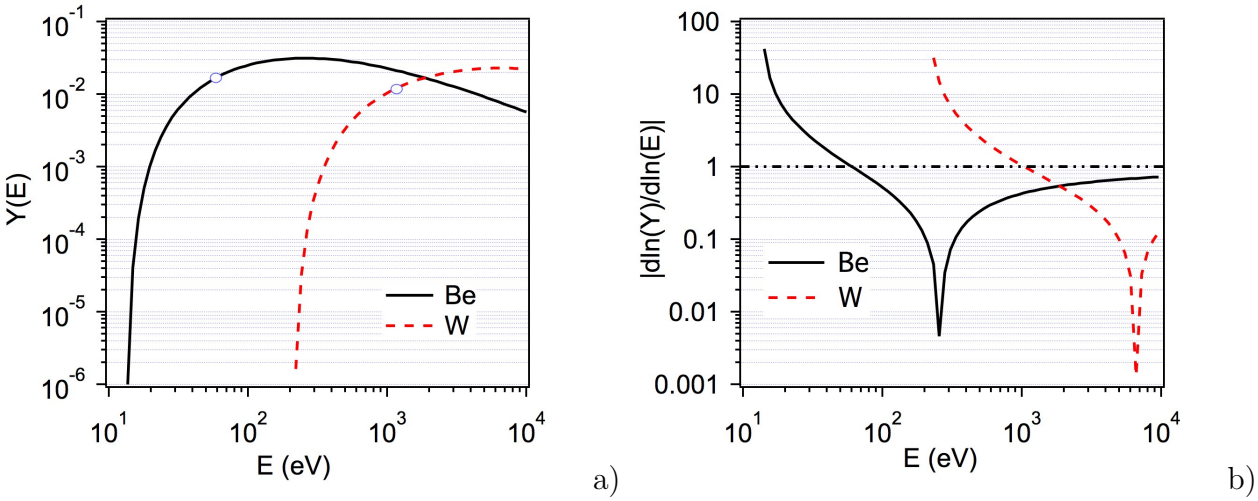

Figure 1. a) Sputtering yield as a function of impinging ion energy in eV for D on Be (solid black) and W (dotted red). b) Fluctuation amplification factor (see text) for Be (solid black) and W (dotted red) sputtering as a function of energy. The cusps correspond to the maxima of the sputtering yield, where the latter is locally insensitive to energy fluctuations.

prescription for the impact energy of an ion of charge Z is $E = 2T_i + 3ZT_e$ (see Ref. [21], p. 97), where $2T_i$ accounts for the kinetic energy of the ions at the sheath entrance and $3ZT_e$ for the sheath acceleration. The sheath electrostatic potential drop of $3T_e$ is such that the electric current is zero at the wall. In SOL turbulence, the electrostatic potential ϕ (assuming that the potential of the wall is zero) will fluctuate around this value, so that the proper choice for the energy becomes $E = 2T_i + Z\phi$. As a result, in this mono kinetic approximation, the impact energy is governed by both ion temperature and electrostatic potential fluctuations. This also suggests that the largest the charge Z of the ion, the more potential fluctuations become dominant. The sputtered flux is obtained upon multiplying the yield by the incident parallel particle flux $\Gamma_{\mathcal{P}} = nc_s \cos(\alpha_B)$, where $c_s = \sqrt{(T_i + T_e)/m_i}$ is the sound speed, m_i the mass of the fuel ions. and α_B the angle of incidence of the magnetic field line with respect to the normal to the wall (assuming the field line inclination is such that the parallel contribution dominates). The time averaged sputtered flux is then given by

$$\overline{\Gamma_s(\mathbf{r},t)} = \frac{1}{t_{av}} \int_{t-t_{av}/2}^{t+t_{av}/2} Y_{\mathcal{P}\to\mathcal{T}} \left(2T_i(\mathbf{r},t') + Z\phi(\mathbf{r},t')\right) n(\mathbf{r},t') c_s(\mathbf{r},t') \cos(\alpha_B) dt', \quad (5)$$

where t_{av} is the length of the averaging window (such that $t_{av} \gg t_{cor}$, with t_{cor} the correlation time of fluctuations, in order to ensure reliable estimation of the mean). Calculating this flux requires time series of both plasma density n, electrostatic potential ϕ, and temperatures T_i, T_e.

As a first step, let us first consider the mean sputtering yield itself and look at the effects of a fluctuating impinging energy E (because of fluctuating T_i, ϕ). The mean of

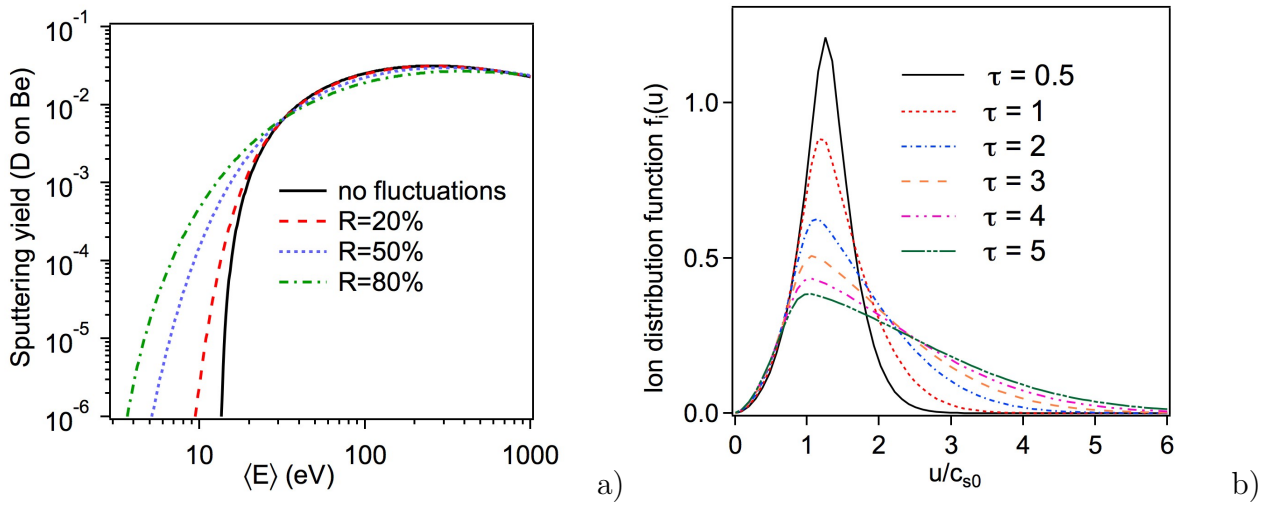

Figure 2. a) mean sputtering yield for D on Be as a function of mean impinging energy in eV, for gamma distributed fluctuations with R=20% to 80%. The black solid line is the pure mono kinetic case (no fluctuations). b) Velocity distribution at the magnetic pre-sheath entrance calculated using the model of Ref. [22], as a function of $u_\parallel/c_{s0}$, for different values of $\tau = T_i/T_e$. Here c_{s0} is the cold ion sound speed, namely $c_{s0} = \sqrt{T_e/M_i}$.

the sputtering yield can be calculated from

$$\langle Y(E)\rangle = \int_0^{+\infty} dE\ W(E)Y(E), \tag{6}$$

where $W(E)$ is the Probability Distribution Function (PDF) of fluctuations, which we here take as a gamma distribution, namely

$$W(E) = \frac{1}{\Gamma_e(\beta)\alpha^\beta} E^{\beta-1} \exp\left(-\frac{E}{\alpha}\right), \tag{7}$$

where α and β are such that $\langle E\rangle = \alpha\beta$ and $\sigma_E^2 = \langle E^2\rangle - \langle E\rangle^2$, and Γ_e is Euler's gamma function. The relative fluctuation level $R = \sigma_E/\langle E\rangle$ is given by $R = 1/\sqrt{\beta}$. As already explained in some of our previous works (see e.g. Ref. [23]), the gamma distribution provides a convenient model for positive random variables. Moreover, several groups have reported that density fluctuations in the SOL have PDF quite close to the gamma distribution (e.g. [24]), and the results from the 2D turbulence model presented in Sec. 3 suggest that the gamma distribution is a reasonable assumption for the other fields too. The average sputtering yields are plotted on Fig. 2 a), for D on Be and fluctuation levels R ranging from 0 (no fluctuations) to 80 %. The effect of fluctuations is reminiscent of that observed on ionization rate coefficients in Ref. [25]: significant sputtering occur at mean temperatures lower than expected because of positive temperature fluctuations. These results are in accordance with Fig. 2 b) which show that the fluctuation amplification factor F is large at near threshold energies. Several additional important qualitative results can already be obtained from this simple model:

i) the fluctuation level must be of the order of several tens of percents for the effects to be significant ii) close to the maximum of the sputtering yield, fluctuations reduce sputtering (because temperature fluctuations around the mean, either positive or negative, lower the yield). Now, while these observations provide a reasonable qualitative understanding of the effects of turbulent fluctuations on sputtering, several additional effects have to be accounted for in order to make a more accurate assessment of the actual magnitude of these effects. First of all, fluctuating fields are correlated and fluctuations in the sputtering yield may be compensated or amplified by fluctuations of the impinging particle flux (nc_s in Eq. 5). In order to take this into account, that is the fact that both density, potential, temperatures fluctuate, we will rely on the TOKAM-2D code described in the next section. But before that, it should be noted that the energy of impinging ions fluctuates even in a quiescent plasma, because of thermal motion. As a result, the first step in improving the model is to introduce a reasonable ion distribution function, especially because we are interested in the near threshold region [21].

To proceed, we model the ion velocity distribution at the magnetic pre-sheath entrance (MPSE) $f_\parallel(u_\parallel)$ by a distribution obtained from a kinetic code [26], which is plotted on Fig. 2 b) for several values of the parameter $\tau = T_i/T_e$. The distribution in the perpendicular direction (2 degrees of freedom) is assumed to be Maxwellian with temperature T_i, so that the mean perpendicular kinetic energy is $E_\perp = 2T_i/2 = T_i$. The parallel and perpendicular directions are thus assumed to be decoupled. The impact energy is then given by $E = \frac{1}{2}m_i(u_\parallel^2 + u_\perp^2) + Z\phi(\mathbf{r},t)$, and the time averaged sputtered flux becomes

$$\overline{\Gamma_s(\mathbf{r},t)} = \frac{1}{t_{av}} \int_{t-t_{av}/2}^{t+t_{av}/2} Y_f\left(\mathbf{r},t'\right) n(\mathbf{r},t') c_s(\mathbf{r},t') \cos(\alpha_B) dt', \tag{8}$$

with

$$Y_f(\mathbf{r},t) = \int_0^{+\infty} du_\parallel f_\parallel(u_\parallel) \int_0^{+\infty} du_\perp f_\perp(u_\perp) Y\left(\frac{1}{2}m_i\left(u_\parallel^2 + u_\perp^2\right) + Z\phi(\mathbf{r},t)\right), \tag{9}$$

where $f_\parallel$ and $f_\perp$ are functions of $\mathbf{r}, t$ through the temperature fields. Here $f_\perp$ stands for the distribution function of the modulus of the perpendicular velocity $\mathbf{u}_\perp$, which is a Rayleigh distribution, namely

$$f_\perp(u_\perp) = \frac{m_i u_\perp}{T_i} \exp\left(-\frac{m_i u_\perp^2}{2T_i}\right). \tag{10}$$

Eq. (9) can be rewritten as

$$Y_f(\mathbf{r},t) = \int_0^{+\infty} dK\, f_{th}(K;\mathbf{r},t) Y\left(K + Z\phi(\mathbf{r},t)\right), \tag{11}$$

where $f_{th}(K;\mathbf{r},t)$ is the kinetic energy distribution at the sheath entrance, at point $\mathbf{r}$ and time t, defined by

$$f_{th}(K) = \int_0^{+\infty} du_\parallel f_\parallel(u_\parallel) \int_0^{+\infty} du_\perp f_\perp(u_\perp) \delta\left(K - \frac{1}{2}m_i\left(u_\parallel^2 + u_\perp^2\right)\right). \tag{12}$$

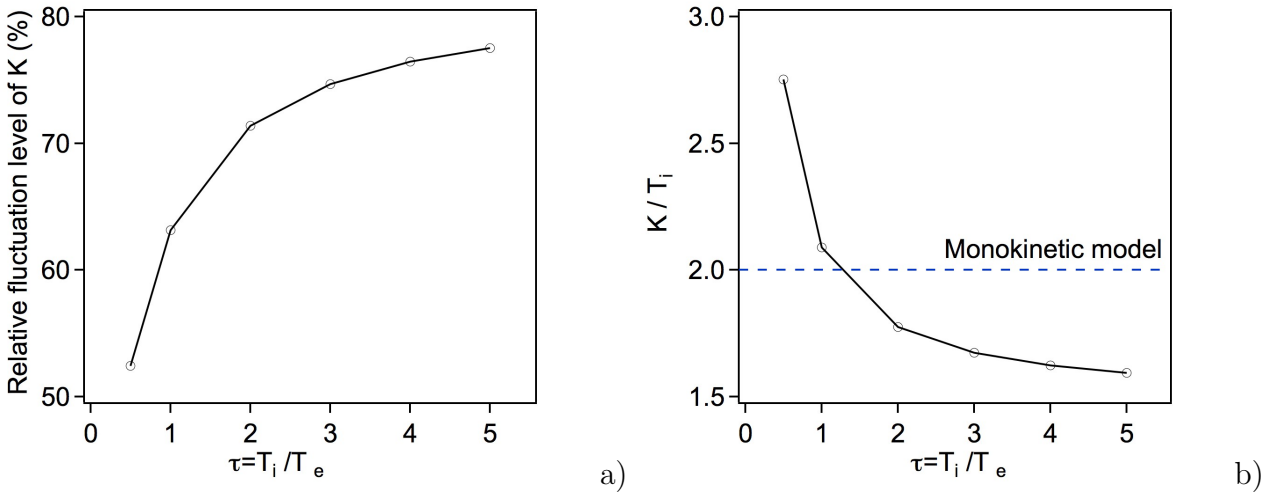

Figure 3. a) Relative fluctuation level of the kinetic energy of ions at the MPSE, due to thermal motion. b) Proportionality factor between the mean kinetic energy and T_i.

It is instructive to calculate the fluctuation level of the kinetic energy, originating from the microscopic velocity dispersion of ions, in order to compare it to fluctuation levels of turbulence (in particular to that of ϕ, see Eq. 9). The moments $M_n = \int dK K f_{th}(K)$ $(n > 0)$ of the distribution f_{th} are easily calculated, namely

$$M_n = \int_0^{+\infty} du_\parallel f_\parallel(u_\parallel) \int_0^{+\infty} du_\perp f_\perp(u_\perp) \left[\frac{1}{2} m \left(u_\parallel^2 + u_\perp^2\right)\right]^n . \tag{13}$$

The kinetic energy fluctuation level, R_K, is given by $\sigma_K = \sqrt{M_2 - M_1^2}/M_1$, and depends only on $\tau = T_i/T_e$ (which controls the shape of the distribution for $u_\parallel$, see Fig. 2 b). In the perpendicular direction, where velocities are distributed according to the Rayleigh distribution, Eq. (10), we have $\sigma_\perp = \sqrt{(4-\pi)/\pi} \simeq 52\%$. σ_K is plotted against τ on Fig. 2 a), and goes up to 80 % for the values of τ considered here. The increase with τ is consistent with the changes in shape of $f_\parallel$ observed on Fig. 2 b). We shall see in the following that these fluctuation levels are larger than those characterizing turbulent fields, and this already suggest that these effects cannot be ignored in our work. Another point of interest when comparing this refined model to the monokinetic model is the value of K/T_i (2 in the mono kinetic case, where $E = K + 3T_e = 2T_i + 3T_e$). This ratio is plotted as a function of τ on Fig. 2 b), and is shown to vary between roughly 2.7 and 1.6 in the range of τ considered here. On the one hand, these values stay rather close from 2, which shows that the models are reasonably coherent, but one the other hand this has to be kept in mind when comparing results obtained from the two models. In fact, differences in mean sputtering yields will not only be related to averaging non-linear functions, but also to the fact that the mean energies are not exactly the same. In the following, we choose not to correct for this effect, because the assumption that $E = 2T_i + 3T_e$ is often used in the literature. The sputtering yields obtained from the two models are plotted as a function of the electron temperature on Fig. 7, which clearly shows that accounting for the ion velocity distribution makes a large difference

in the threshold region, as expected.

In the following, we will assess the effects of turbulence on both models, but in view of Eq. (5) and (8), this requires accounting for the simultaneous effects of density, temperatures and potential fluctuations. In order to address this point, we will rely on the TOKAM-2D code described below. Although its physics model does not capture all the possibly relevant effects (in particular finite wavenumber $k_\parallel$ of the fluctuations in the parallel direction, since it relies on the flute approximation), we think the results provide a sound starting point for our purposes. Indeed, one could have built a joint gamma PDF for the various fields involved, (see [27]) and proceed in the spirit of our previous works. However, with 4 different fields involved the parameter space becomes quite large and the simulation results can be seen as an attempt to restrict that parameter space. It should also be kept in mind that the Bohdansky formula has a limited accuracy, and that many other ill-controlled parameters will contribute to set the actual sputtering yield: for instance ion incidence angles, accounting for surface roughness, chemical composition of the surface (for a recent example, see Ref. [28]). Therefore, in this work we are looking for semi-quantitative results, that is, correctly identifying the qualitative effect of fluctuations and giving an estimate of the size of their contribution. We think that the turbulence model to be presented in the next section is complete enough in view of our goals here.

3. The non-isothermal TOKAM-2D code

The results presented in this section are obtained using the bi-dimensional fluid code TOKAM-2D [29]. It models turbulence generated by the interchange instability SOL region of tokamaks. Perpendicular velocities are derived in the drift ordering. The flute hypothesis ($k_\parallel = 0$) is used to reduce the model from 3D to 2D. Under this assumption, parallel transport is described by loss terms due to boundary conditions which are computed using Bohm sheath conditions. A new version, including the evolution of both electron and ion intern energies has been recently developed to study the impact of ion energy on edge transport. A set of four coupled equations is solved by TOKAM-2D: electron density balance, charge balance, electron and ion energy balances. The geometric configuration is slab, $x = (r - a)/\rho_L$ and $y = a\theta/\rho_L$ are respectively the radial and poloidal directions with ρ_L the ion Larmor radius and a the tokamak minor radius. More details about model derivation and normalizations can be found in [29]. Finally, the four conservation equations solved are

$$\partial_t N + [\phi, N] - D_N \nabla_\perp^2 N = S_N - \sigma N \sqrt{T_e + T_i} \exp\left(\Lambda - \frac{\phi}{T_e}\right) \tag{14}$$

$$\partial_t W + [\phi, W] - \nu \nabla_\perp^2 W = -\frac{g}{N} \partial_y (P_e + P_i) + \sigma \sqrt{T_e + T_i} \left(1 - \exp\left(\Lambda - \frac{\phi}{T_e}\right)\right) \tag{15}$$

$D_N = \nu = \chi_e = \chi_i$	σ	g	Λ	γ_e	γ_i	T_e^{in}	T_i^{in}
5×10^{-3}	10^{-4}	6×10^{-4}	2.8388	4	2.5	3	1

Table 2. Set of parameters used for TOKAM-2D simulations.

$$\partial_t \frac{3}{2} P_e + \frac{3}{2}[\phi, P_e] - \frac{3}{2}\chi_e \nabla_\perp^2 P_e = T_e^{in} S_N - \gamma_e \sigma P_e \sqrt{T_e + T_i} \exp\left(\Lambda - \frac{\phi}{T_e}\right) \quad (16)$$

$$\partial_t \frac{3}{2} P_i + \frac{3}{2}[\phi, P_i] - \frac{3}{2}\chi_i \nabla_\perp^2 P_i = T_i^{in} S_N - \gamma_i \sigma P_i \sqrt{T_e + T_i} \quad (17)$$

where $[\phi, \cdot] = \partial_x \phi \partial_y \cdot - \partial_y \phi \partial_x \cdot$ corresponds to the Poisson bracket representing advection by $E \times B$ drift velocity. N, ϕ and $W = \nabla_\perp^2 \phi + \boldsymbol{\nabla}.(\frac{1}{N}\boldsymbol{\nabla}_\perp P_i)$ are respectively the electron density, the electrostatic potential and the generalized vorticity. One can notice the contribution of the ion pressure within the vorticity formulation in comparison with the more conventionally used cold ions model. D_N, ν, χ_e and χ_i are transverse dissipative coefficients representing respectively diffusion, viscosity, electron and ion heat conductions. The sheath conductivity $\sigma = \rho_L / L_\parallel$ and the electron and ion sheath heat transfer coefficients γ_e and γ_i control the sheath parallel losses. Concerning these parallel losses, the term $\exp(\Lambda - \frac{\phi}{T_e})$, where $\Lambda = \frac{1}{2}\ln\frac{m_i}{2\pi m_e}$ is the normalized sheath potential drop, corresponds to the screening effect of slow electrons by the sheath. The terms $\sqrt{T_e + T_i}$ represent the temperature dependency of the normalized parallel acoustic velocity. The term involving g, the magnetic field lines curvature coefficient, is the driver of the interchange instability and the only curvature term retained in our model for ordering and simplicity considerations. The flux-driven approach of the model is ensured by a time- and poloidally-constant gaussian density source S_N. This source represents the forcing particule flux coming from the core plasma by perpendicular transport. T_e^{in} and T_i^{in} are the temperatures of incoming electrons and ions associated with the source term S_N. The set of parameters used in the TOKAM-2D simulations are displayed in Table 2. The latter correspond to standard values of SOL plasmas in a medium size tokamak like Tore Supra.

4. Properties of SOL fluctuations

This section aims at describing turbulence properties in the SOL. We focus on properties relevant for the remainder of this study, thus this description shall not be considered as an exhaustive characterization of SOL turbulence. These main relevant parameters are the electrostatic potential ϕ, the ion temperature T_i and the parallel particle flux at the sheath entrance $\Gamma_\parallel = N c_s$. We characterize the fluctuations of these three fields and then study their phase relatively to each other. We first describe the global behavior of the relevant fields in the simulation box, whose size is $256\rho_L \times 256\rho_L$. The radial profiles (time and poloidally averaged) of the parallel particle flux, ion temperature and electrostatic potential are plotted on Figure 4 a). In this simulation, the particle source is a Gaussian centered at $x = 10$ with a standard deviation $\sigma = 8$. One can observe

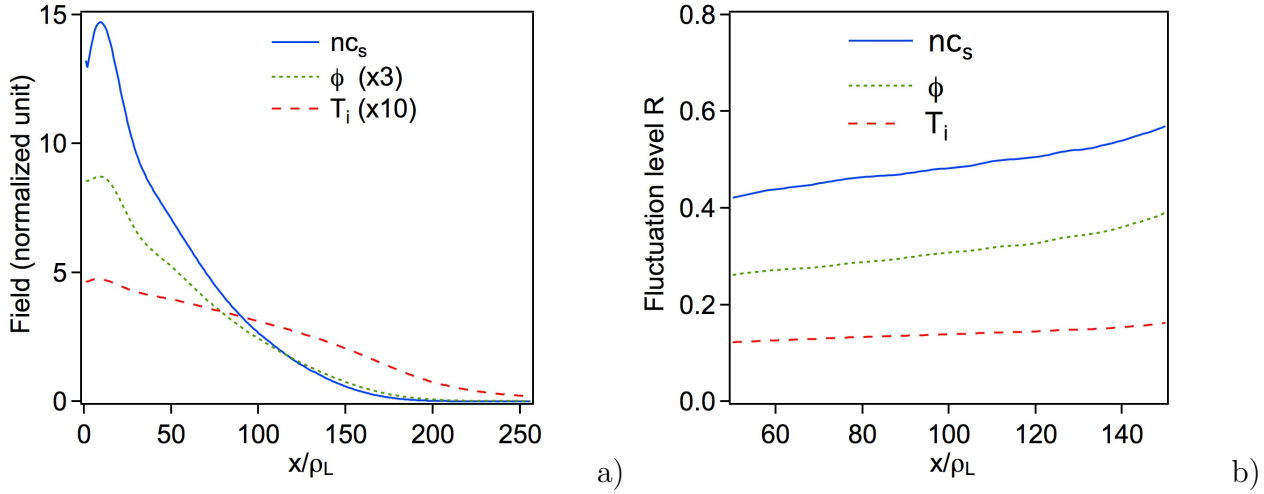

Figure 4. a) Radial profiles of time- and poloidally averaged parallel flux $< \Gamma_{\parallel} >_{t,y}$, ion temperature $< T_i >_{t,y}$ and electrostatic potential $< \phi >_{t,y}$ for $T_e^{in} = 3$ and $T_i^{in} = 1$. b) Radial profiles of relative fluctuation levels of parallel flux $\Gamma_{\parallel} = Nc_s$, ion temperature T_i and electrostatic potential ϕ for $T_e^{in} = 3$ and $T_i^{in} = 1$.

three different radial regions. First, from $x = 1$ to $x = 50$, the region where the source shape has a strong influence on the radial profiles. On the opposite side of the box, for $x = 150$ to $x = 256$, we observe a region where the box is almost empty of particles and energy, in which the model starts to reach its limits. Between these two regions, profiles do not have any external constraints. In the remainder of this study, we focus on this radial area between $x = 50$ and $x = 150$. The radial profiles of relative fluctuation levels are presented in Figure 4 b) for the parallel particle flux, the ion temperature and the electrostatic potential for a simulation where the electron injection temperature T_e^{in} is three times larger than the ion injection temperature T_i^{in}. These values have been chosen in order to have realistic ratios of ion and electron temperatures in the SOL [30]. These fluctuations have been normalized to the time- and poloidally averaged value of the corresponding fields. One can observe that the fluctuation levels are around 50% for the parallel particle flux, 30% for the electrostatic potential and only 12% for the ion temperature. These differences can be interpreted as follows. First, the parallel particle flux $\Gamma_{\parallel}$ involves simultaneously density, electron and ion temperatures (through the parallel acoustic velocity), which can explain the comparatively large fluctuations level of the parallel particle flux, provided the fluctuations of these fields have cumulative effects, i.e. are broadly in phase. That this is indeed true will be shown below. For electrostatic potential fluctuations, one can notice that the parallel dynamic tends to peg ϕ to ΛT_e, so that the fluctuations of ϕ and T_e behave in a very similar way. Finally, the gap in relative fluctuation level between ϕ (and thus T_e) and the ion temperature can be explained by the fact that losses in the parallel direction are lower for ion energy than for electron energy, so that larger electron temperature gradients develop, hence larger relaxation events. The fluctuation levels obtained in TOKAM-2D are next compared to experimental observations in the SOL. For the parallel particle flux, measurements are

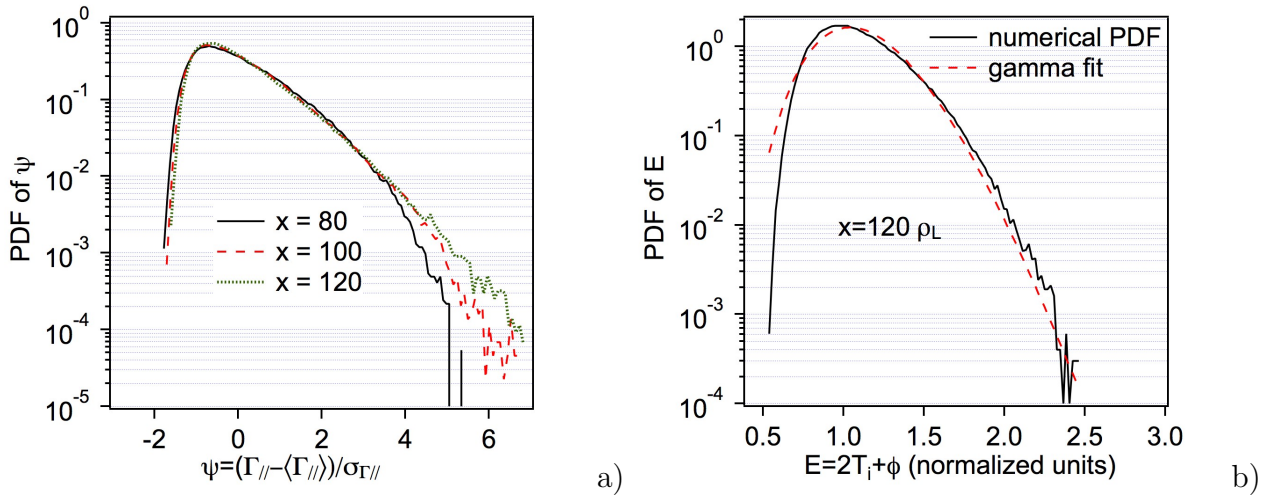

Figure 5. a) PDF of $(\Gamma_\parallel - <\Gamma_\parallel>)/\sigma_{t,y}(\Gamma_\parallel)$ for several radial positions. b) Centered and normalized PDF of ion impact energy $E = 2T_i + \phi$ (mono kinetic model) at $x = 120$ together with the corresponding gamma distribution.

in good agreement with TOKAM-2D non-linear simulations. For example, a relative fluctuation level of saturation current between 30 and 50% is found on Alcator C-Mod [31]. Density fluctuation levels around 40% are also found in D-IIID in L-mode plasmas [32]. Things get more complicated for the electrostatic potential and ion temperature fluctuations. Indeed, experimental data are still quite scarce, and the few available datasets span a fairly broad range of values, and are moreover sometimes at least apparently contradictory. In fact, the level of fluctuations for ion temperature ranges from 10% [33] to 400% [34]. Care has to be taken that some measurement are made close to the separatrix while others pertain to the far SOL. Moreover, the level of fluctuations is sometimes normalized to the mean value, as in our study, or to the background plasma (that is, the inter-filament value) which naturally leads to higher fluctuation levels. One can only say that the fluctuation levels obtained for the electrostatic potential and the ion temperature in our non-linear simulations are in the lower range of experimental observations. Finally, we observe that the fluctuations levels are slightly increasing radially for all fields $\Gamma_\parallel$, ϕ and T_i. This increase is larger for the parallel particle flux (from 42% at $x = 50\rho_L$ to 57% at $x = 150\rho_L$) and the electrostatic potential (from 26% at $x = 50\rho_L$ to 39% at $x = 150\rho_L$) than for the ion temperature (from 12% at $x = 50\rho_L$ to 16% at $x = 150\rho_L$).

In order to better characterize the fluctuations, we turn our attention to probability density functions (PDFs). The tails of the PDFs are of particular interest for our purposes, because they measure the probability of occurrence of large fluctuations, which are likely to play a key role in a possible sputtering enhancement by turbulence. On Fig. 5 a), the probability density function of parallel particle flux fluctuations normalized to the standard deviation, $(\Gamma_\parallel - <\Gamma_\parallel>_{t,y})/\sigma_{t,y}(\Gamma_\parallel)$, are plotted for three radial positions: $x = 80$, $x = 100$ and $x = 120$. The PDFs are clearly positively skewed, which

means that large amplitude events make a substantial part of the mean parallel flux. The skewness of this centered PDF seems to be slightly increasing radially, together with the fluctuation level. This result is consistent both with experimental observations [32] and 3D non-linear codes results, e.g. TOKAM-3X [35] and GEMR [36]. A similar behavior is also obtained for the normalized PDFs of ϕ, while the normalized PDF of ion temperature fluctuations appears to be quasi-symmetric, i.e with an almost-zero skewness. Fig. 5 a) shows the PDF of the kinetic energy of ions at the wall, in the mono kinetic model, i.e. $E = 2T_i + \phi$. The PDF is found to be close to a gamma distribution Eq. (7), giving ground to the choice which was made in Sec. 2 for $W(E)$. The parameters α and β from the gamma distribution are obtained from the time series, and are not further adjusted to improve agreement.

We finally focus on the phase shift between electrostatic potential, parallel particle flux and ion temperature fluctuations as this will determine their combined impact on non-linear terms related to sputtering. The radial profiles of phase shift between $\Gamma_\parallel$, ϕ and T_i are plotted in Figure 6 a).The phase shifts are computed using the formula

$$\theta(F_1, F_2) = \cos^{-1}\left(\frac{< \tilde{F}_1 \tilde{F}_2 >_{t,y}}{\sqrt{< \tilde{F}_1^2 >_{t,y} < \tilde{F}_2^2 >_{t,y}}}\right), \tag{18}$$

with $\tilde{F} = F - < F >_{t,y}$. The phase shift is around $\pi/5$ between the parallel particle flux and the ion temperature at all radii. It reaches approximatively $\pi/4$ (resp. $\pi/3$) at $x = 50$ for the phase shift between the electrostatic potential and the parallel particle flux (resp. the ion temperature). The phase shifts seem to decrease radially, especially between the electrostatic potential and the two other fields. This radial variation can probably be explained by changes in the relative weights of the instabilities driving fluctuations in the model, as pointed out in Ref. [37]. In order to get a better understanding of what the phase shift between the relevant fields mean, a conditional averaging technique is used (taking into account only large parallel flux events, with an amplitude larger than $< \Gamma_\parallel >_{t,y} + 2\sigma_{\Gamma_\parallel}$ at $x = 120$). The poloidal shape of the three studied fields are computed during these large events and presented on the Figure 6 b). The parallel particle flux is the reference curve with thus a zero poloidal delay. Its shape is close to a Gaussian function and has a poloidal extension of about $20\rho_L$. The ion temperature is in phase poloidally with the parallel flux. For the electrostatic potential, one can observe a poloidal shift of the distribution peak by 4-5ρ_L in comparison to the peaks of parallel flux and ion temperature. This shift is the evidence of a poloidal phase shift between the electrostatic potential and the two others fields. However, this phase shift is moderate, the three fields are definitely quite well in phase.

5. Mean Sputtered fluxes and yields

We now make use of the numerical simulations described in the previous section in order to compute mean sputtering yields and fluxes, as a function of a measure of the

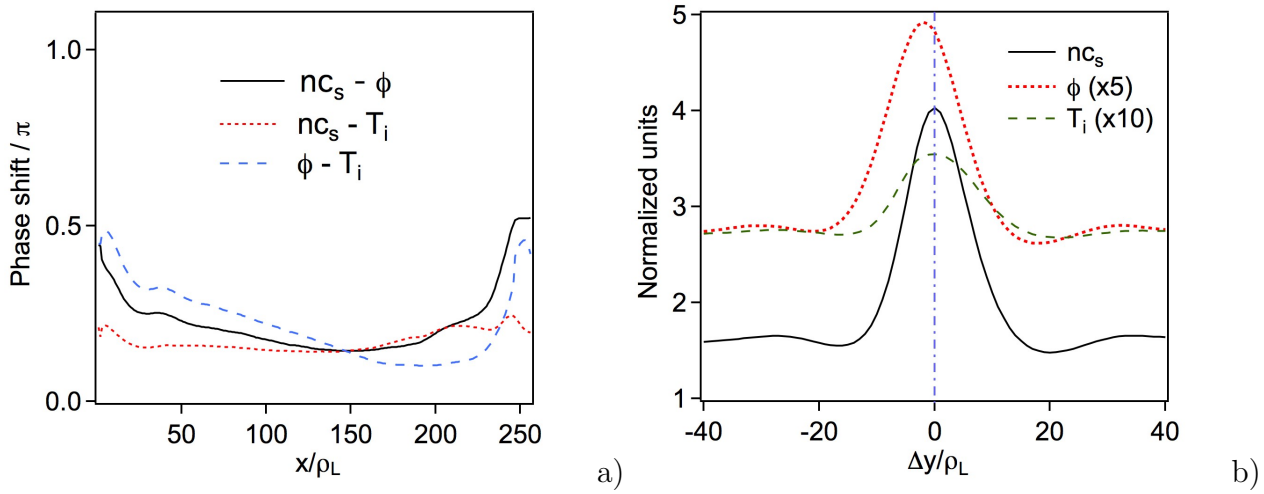

Figure 6. a) Radial profile of phase shift between the parallel flux $\Gamma_\parallel$, the ion temperature T_i and the electrostatic potential ϕ for $T_e^{in} = 3$ and $T_i^{in} = 1$ b) Poloidal shape of $\Gamma_\parallel$, ϕ and T_i at $x = 120$ during large parallel flux events obtained with conditional averaging. The amplitude of electrostatic potential and ion temperature are artificially increased respectively by a factor 5 and 10 in order to simplify comparison.

mean impinging energy $\langle E \rangle$. It is customary to plot measured sputtering yields as $E_m = 2\langle T_i \rangle + 3Z\langle T_e \rangle$, or even simply $\langle T_e \rangle$. The link between these various measures of the impinging energies will depend on the properties of the fluctuating fields ($\langle \tau \rangle$ in particular), and complicate matters when comparing experiments to models.

In order to vary the mean temperature, we keep all reference values constant (in particular the reference temperature T_0 to which all temperatures are normalized), and vary the injection temperatures T_e^{in} and T_i^{in} (that is, the ratio between the energy and the particle sources). In this way, the size of the simulation domain remains constant throughout the power (hence mean temperature) scan. In the following we take $T_0 = 100$ eV and $n_0 = 10^{18}$ m^{-3}. The value of the ratio T_e^{in}/T_i^{in} allows changing $\tau(x) = \langle T_i \rangle / \langle T_e \rangle$. However the mean value of the later also depends on the completion between parallel and radial transport, and thus on the radial position. In the following we set $T_e^{in}/T_i^{in} = 3$, in accordance with the simulations presented in the previous section. Simulations are run for T_e^{in} ranging from 1 to 12 (non-dimensional units). We calculate yields using time series at radial position $x = 128\rho_L$. The mean value of $\tau = T_i/T_e$ is plotted on Fig. 7. The error bars give the standard deviation of τ for these simulations. Fig. 7 b) compares the sputtering yields calculated using mean fields in the monokinetic approximation and the thermal averaging procedure described in Sec. 2, plotted as a function of $\langle T_e \rangle$. As said earlier, care should be taken in comparing these results since for given values of $\langle T_e \rangle$ and $\langle T_i \rangle$, the mean kinetic energy of ions at the MPSE, K, is not the same in the two models. In particular, as shown on Fig. 2 b), $K > 2T_i$ for the thermally averaged model for $\langle T_e \rangle \leq 20eV$, at least partially explaining the higher sputtering yields in the low temperature range (the remainder of the effect being related to averaging a non

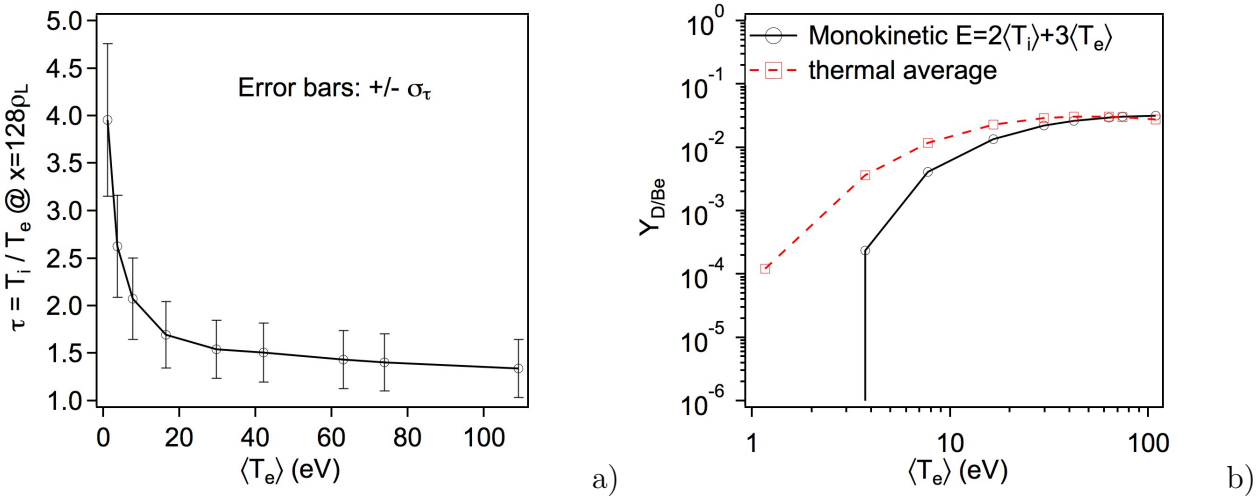

Figure 7. Sputtering yields for D on Be calculated using mean fields values in the simulations, at $x = 128\rho_L$ for the mono kinetic model (back solid line) and for the thermally averaged model (dashed red line)

linear function of the energy).

We now focus on the effects of fluctuations. The mean value of the sputtering yields $\langle Y \rangle$ is compared to the sputtering yield calculated for the mean fields $Y(\langle\phi\rangle, \langle T_e\rangle, \langle T_i\rangle)$ (as would be done in a mean field, i.e. transport, code) on Fig. 8 a) (monokinetic model) and c) (thermally averaged model). As anticipated from the simple calculations of Sec. 2 based on a gamma distribution for the impact energy E, fluctuations do increase sputtering at near threshold temperatures. In the mono kinetic model, at the threshold sputtering is increased by a factor of 2. For these temperatures, the yield is typically 30 times lower than its maximum value. The effects are weaker for the thermally averaged model, as expected, where the sputtering yield increases by a factor of 2 for the lowest mean temperature value available (but at this temperature the yield is typically 2 orders of magnitude lower than at its maximum). Fig. 8 b) and d) show the corresponding results for the sputtered fluxes, for which the effects of fluctuations is slightly stronger, because as shown in the previous section (see Fig. 6, at $x = 128\rho_L$) the particle flux is quite well in phase with temperatures and potential fluctuations. Overall, the results of the simulations presented here show modest effects, not because of cancelation between fluctuations of the different fields (since the phase shifts are quite low, of the order of $\pi/5$, see Fig. 6 a)), but presumably rather because of the values of the fluctuation levels of ion temperature and potential (respectively $\simeq 15\%$ and $\simeq 30$ % at $x = 128\rho_L$, see Fig. 4). Moreover, the results look similar for yields and fluxes, but parallel flux fluctuations strengthen the effects observed on fluxes, since they are again essentially in phase with temperature and potential fluctuations.

In order to assess the role of the fluctuation level, which is not strongly constrained experimentally at the time of writing as discussed before, we choose to alter

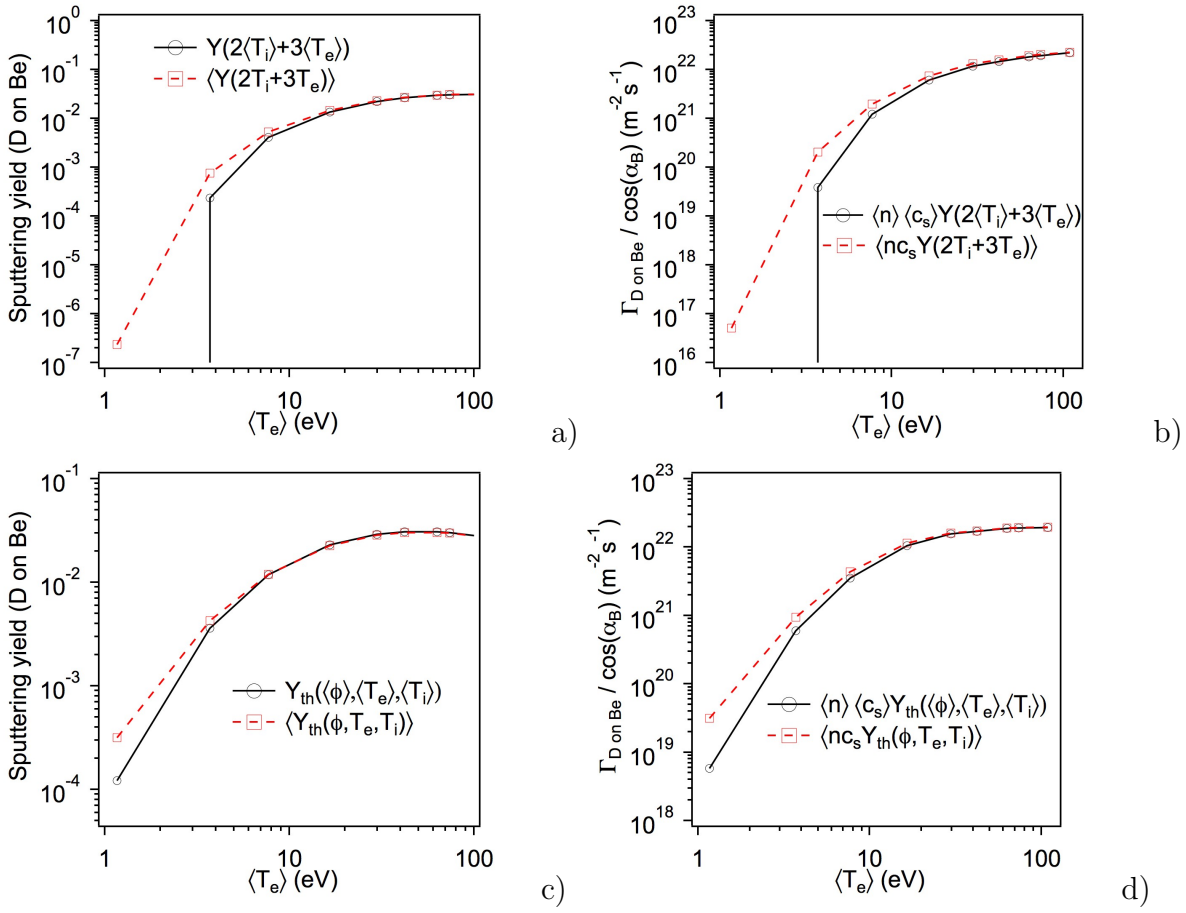

Figure 8. Sputtering yields (D on Be) and sputtered fluxes for the mono kinetic model a), b) and the thermally averaged model c) and d). α_B is the angle between the magnetic field line and the normal to the wall.

the TOKAM-2D time series in order to increase R. In order to do so, for a given field X with fluctuation level R, we calculate the fluctuations around the mean $\delta X = X - \overline{X}$, and then construct a new time series X' such that $X' = \overline{X} + \eta\delta X$, with $\eta > 0$. It is straightforward to check that the relative fluctuation level of the new time series is given by $R' = \sqrt{\overline{(\delta X')^2}}/\overline{X'} = \eta R$. In fact, for positive fields such as temperature and density we use $X' = \max(\overline{X} + \eta\delta X, X_{min})$ with $X_{min} = 0.1$ in non-dimensional units. For large fluctuation levels, this could introduce a significant bias (since for instance $\overline{X'} \geq \overline{X}$), but in cases studied here the bias is small enough in order not to affect our conclusions. In order for $\tau = T_i/T_e$ to remain in a reasonable range, we make a further assumption. The ion temperature is modified according to the procedure just described, and the electron temperature is redefined as $T_e(t) = \overline{\tau}/T_i(t)$ where $\overline{\tau}$ is calculated from the initial time series. Because of this, the results obtained for $\eta = 1$ are somewhat different from the original ones, shown on Fig. 8, and turn out to underestimate the effects of fluctuations. The effect of increasing η, hence the fluctuation level, are shown on Fig. 9 for yields and fluxes. Both n, T_i and ϕ are modified. Their initial fluctuation level, for the case such

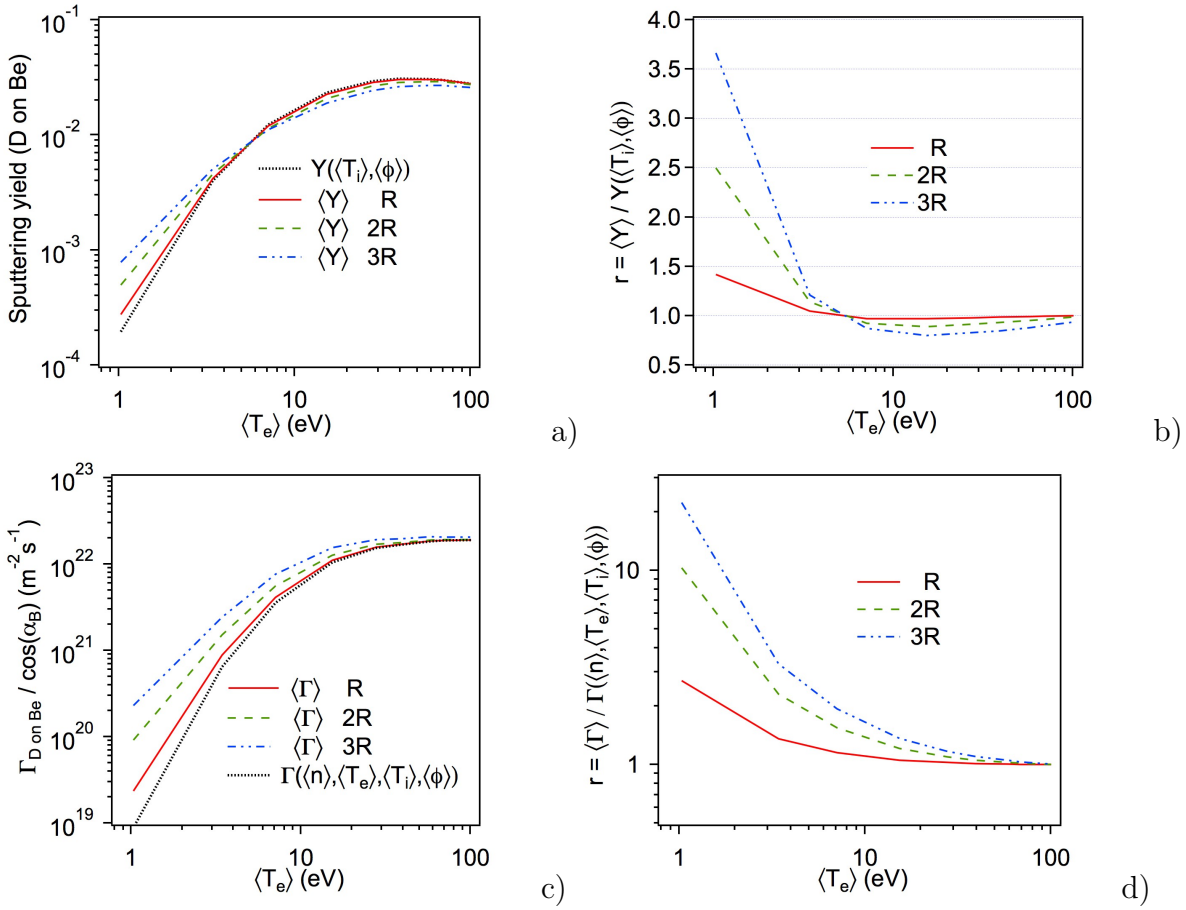

Figure 9. Sputtering yields (D on Be) a) and sputtered fluxes c) for the thermally averaged model, and the ratio of the mean flux to the yield b) and sputtered flux d) as a function of the mean electron temperature, using a constant value for τ, for different values of the fluctuation levels (artificially increased by a factor of 2 and 3). α_B is the angle between the magnetic field line and the normal to the wall.

that $\langle T_e \rangle = 20$ eV at $x = 128\rho_L$, can be read from Fig. 4 b) for T_i and ϕ (respectively around 15 and 30 %), and for n we have 35%. These values have to be multiplied by $\eta = 2$ and 3 for the cases labelled by $2R$ and $3R$. The fact that the size of the effects increase with fluctuation level is clear, and is made more quantitative on Fig. 9 where the ratio between the mean sputtering yields/fluxes to the yield/fluxes calculated with the mean fields is plotted. The latter shows a behavior very similar to the one observed previously for ionization rate coefficients [38], which is not surprising since the temperature dependence of the two quantities is quite the same. Typically, for large fluctuation levels (of order unity), one can expect more than an order of magnitude increase of the sputtered flux, in a temperature domain where the yield is between one and three orders of magnitude below its maximum. Overall, we can thus conclude that fluctuations can significantly increase sputtering with respect to mean fields estimations, all the more so that the energy is low. In other words, the increase becomes more and more marked as sputtering becomes less and less important. Therefore, fluctuation enhanced sputter-

ing could have deleterious consequences on long discharges, either for fuel retention in ITER because of Be codeposition, or for W contamination in a full W DEMO. Sputtering enhancement is likely to be relevant for the low field side part of the first wall, because of the balloonned character of SOL turbulence [39, 35]. One possible way of retaining these effects in mean field codes would be to rely on effective, or "fluctuation dressed", sputtering coefficients defined as $Y^{eff}_{\mathcal{P}\rightarrow\mathcal{T}} = \langle\Gamma_{\mathcal{P}\rightarrow\mathcal{T}}\rangle/(\langle n\rangle\langle c_s\rangle\cos(\alpha_B))$, but the latter would not only depend on the values of the mean fields but also on the relative fluctuation levels and correlations of all the fields (n, ϕ, T_e, T_i). The fact that all fields seem to be roughly in phase simplify matters, but whether the number of parameters can be reduced to a manageable one remains to be investigated. This could involve a simplified turbulence model from which fluctuation levels could be inferred from the mean fields and their gradients.

Two additional important points remain to be highlighted before concluding. First, prompt redeposition has been neglected because it is thought to be immaterial, even for W, on the first wall where mean densities and temperatures are low (hence W atoms do have mean free path typically larger than the W^+ ion gyroradius), see e.g. Ref. [9]. The situation would be different in the divertor, and if significant fluctuations occur there estimations of the mean sputtered flux would have to take the redeposited fraction into account. In the simplest model [40], the non-redeposited fraction is given by $p^2/(1+p^2)$, where $p = \omega_{ci}\tau^{io}_W$, with ω_{ci} the ion gyro frequency and τ^{io}_W the ionization time of W, which has a strong temperature dependence below 30 eV. It is likely that taking prompt deposition into account would make the flux of W atoms effectively released in the plasma less sensitive to fluctuations, since positive temperature excursions would simultaneously increase sputtering and redeposition because of shortened mean free paths (note also that positive correlations between temperature and density would also reinforce both mechanisms). However, it should be noted that turbulent density fluctuations affect the stopping power of the plasma [41], especially when the mean free path of atoms is smaller than the correlation length of filaments (typically 1 cm), which is the case for W atoms in these conditions. Obtaining quantitative results would require a dedicated study. Another important question is related to the measurements of sputtered fluxes, for instance by spectroscopy. These measurements generally do not resolve turbulent fluctuations in time, and the effect of the latter on the measurement process remains to be assessed, along the same line as previous works on spectral line shapes [23] and collisionnal-radiative models [42]. This is important in view of ensuring consistency between measurements of the mean plasma parameters and of the sputtered fluxes, and will be the subject of future work.

6. Conclusions

We have discussed the effects of turbulent fluctuations on first wall sputtering, which is a concern especially for future tokamaks such as ITER and DEMO. Elementary

considerations about the non linear dependance of sputtering yields with ion impact energy, which presents a threshold, suggest that fluctuations could very significantly enhance sputtering in low temperature conditions, that is in the threshold region. However, for this type of near threshold sputtering study, a mono kinetic model for impinging ions could lead to misleading results (overestimating the importance of fluctuations), and the ion velocity distribution has to be taken into account. In parallel direction, we have relied on the results of kinetic calculations, the shape of the distribution being parametrized by $\tau = T_i/T_e$. Furthermore, the sputtered fluxes depend both on ion temperature, electron temperature, electrostatic potential and density fluctuations, which are not statistically independent. A newly developed version of the TOKAM-2D code, solving energy equations both for electrons and ions is presented, and time series generated by the code are used to provide estimates of the size of the effect fluctuations have on the mean sputtering yields and fluxes. Results show modest enhancements of yields and fluxes, in particular because relative fluctuation levels are also quite modest, in particular for ion temperature (although not inconsistent with some experimental data in the literature). The various fields are quite well in phase (something also observed on codes based on more complete models), and compensations of the contributions of several fields do not seem to occur. Artificially increasing the fluctuation levels, staying within the broad range of experimentally observed values, leads to enhancements of more than one order of magnitude. We therefore conclude that fluctuations could indeed significantly enhance first wall sputtering, and that more work is needed to assess the influence of fluctuations on spectroscopic measurements as well as on what happens in the divertor where prompt redeposition is strong.

7. Acknowledgements

We are grateful to Dr. J. Gunn for providing us tabulated parallel velocity distributions at the sheath entrance. Financial support from the Agence Nationale de la Recherche (ANR) is acknowledged, though the projects ANR-11-BS09-023 (SEDIBA) and the A*MIDEX project (ANR-11-IDEX-0001-02), the latter being funded by the Investissements d'Avenir French Government program. Finally, part of this work has also been carried out within the framework of the French Research Federation for Fusion Studies, and of the EUROfusion Consortium, and has received funding from the Euratom research and training programme 2014-2018 under grant agreement No 633053. The views and opinions expressed herein do not necessarily reflect those of the European Commission.

[1] A. Loarte et al. Progress in the iter physics basis chapter 4: Power and particle control. *Nucl. Fusion*, 47:S203, 2007.
[2] J. Roth et al. *Plasma Phys. Control. Fusion*, 50:103001, 2008.
[3] R .Pitts et al. *J. Nucl. mater.*, 438:S48, 2013.
[4] A. V. Chankin, D. P. Coster, and R. Dux. *Plasma Phys. Control. Fusion*, 56:025003, 2014.
[5] D. Tskhakaya et al. *J. Nucl. mater.*, 463:624, 2015.

[6] M. Greenwald et al. *Phys. Plasmas*, 21:110501, 2014.
[7] R. Dux et al. *J. Nucl. Mater.*, 390-391:858, 2009.
[8] H. Bufferand et al. *Nucl. Fusion*, 55:053025, 2015.
[9] Y. Marandet et al. *J. Nucl. Mater.*, 463:629, 2015.
[10] A. S. Kukushkin et al. *Nucl. Fusion*, 45:608, 2005.
[11] R. Schneider et al. *Contrib. Plasma Phys.*, 46:3, 2006.
[12] R. Simonini et al. *Contrib. Plasma Phys.*, 34:368, 1994.
[13] S. Wiesen. Edge2d/eirene code interface report. `www.eirene.de/e2deirreport30jun06.pdf`, 2006.
[14] T. Rognlien et al. *J. Nucl. Mater.*, 266-269:654, 1992.
[15] H. Kawashima et al. *Plasma and Fusion Research: Regular Articles*, 46:31, 2006.
[16] S. Brezinsek et al. *Nucl. Fusion*, 54:103001, 2014.
[17] Y. Marandet, J. Rosato, H. Capes, L. Godbert-Mouret, M. Koubiti, A. Mekkaoui, F.B. Rosmej, and R. Stamm. *High Energy Density Phys.*, 5(4):312, 2009.
[18] S. I. Krasheninnikov, A. Yu. Pigarov, T. K. Soboleva, and D. L. Rudakov. *Phys. Plasmas*, 16:014501, 2009.
[19] E. Havlickova et al. *J. Nucl. Mater.*, 415:S471, 2011.
[20] A. Yu Pigarov et al. *Phys. Plasmas*, 18:092503, 2011.
[21] P. C. Stangeby. *The plasma boundary of magnetic fusion devices.* Institute of physics publishing, Bristol and Philadelphia, 2000.
[22] K. S. Chung and I. H. Hutchinson. *Phys. Rev. A*, 38:47, 1988.
[23] Y. Marandet, H. Capes, L.Godbert-Mouret, M. Koubiti, and R. Stamm. *Europhys. Lett.*, 69:531–537, 2005.
[24] J. P. Graves, J. Horacek, R. A. Pitts, and K. I. Hopcraft. *Plasma Phys. Control. Fusion*, 47:409, 2005.
[25] F Guzman, Y Marandet, P Tamain, H Bufferand, G Ciraolo, Ph Ghendrih, R Guirlet, J Rosato, and M Valentinuzzi. *plasma phys. control. fusion*, 57:125014, 2015.
[26] J. P. Gunn. *Phys. Plasmas*, 4:4435, 1997.
[27] Y. Marandet, A. Mekkaoui, D. Reiter, P. Boerner, P. Genesio, J. Rosato, H. Capes, F. Catoire, M. Koubiti, L. Godbert-Mouret, and R. Stamm. *Plasma Phys. Control. Fusion*, 53:065001, 2011.
[28] N. Mellet et al. *Nucl. Fusion*, 54:123006, 2014.
[29] Y. Sarazin and Ph. Ghendrih. *Phys. Plasmas*, 5:4214, 1998.
[30] M. Kocan et al. *Plasmas Phys. Control. Fusion*, 50:125009, 2008.
[31] J. L. Terry et al. *Phys. Plasmas*, 10:1739, 2003.
[32] S. J. Sweben et al. *Plasma Phys. Control. Fusion*, 49:S1, 2007.
[33] H. T. Evensen et al. *Nucl. Fusion*, 38:237, 1998.
[34] M. Kocan et al. *Plasmas Phys. Control. Fusion*, 54:085009, 2012.
[35] P. Tamain et al. *Plasma Phys. Control. Fusion*, 57:054014, 2015.
[36] S. J. Sweben et al. *Phys. Plasma*, 16:082505, 2009.
[37] C. Baudoin et al. *submitted to contrib. plasma phys.*
[38] Y. Marandet, A. Mekkaoui, D. Reiter, P. Boerner, P. Genesio, F. Catoire, J. Rosato, H. Capes, M. Koubiti, L. Godbert-Mouret, and R. Stamm. *Nuclear Fusion*, 51:083035, 2011.
[39] N. Fedorczak et al. *Phys. Plasmas*, 19:072313, 2012.
[40] G. Fussman et al. Proc. 15th int. conf. on plasma physics and controlled nuclear fusion research (seville, spain) vol 2 (vienna: Iaea). `www-naweb.iaea.org/napc/physics/FEC/STIPUB948VOL3.pdf`, 1995.
[41] A. Mekkaoui, Y. Marandet, D. Reiter, P. Boerner, P. Genesio, J. Rosato, R. Stamm, H. Capes, M. Koubiti, and L. Godbert-Mouret. *Phys. Plasmas*, 19:122310, 2012.
[42] F. Catoire, H. Capes, Y. Marandet, A. Mekkaoui, J. Rosato, M. Koubiti, and R. Stamm. *Phys. Rev. A*, 83:012518, 2011.